2011

Microbial reduction of chlorite and uranium followed by air oxidation

Gengxin Zhang
Chinese Academy of Sciences

William D. Burgos
The Pennsylvania State University, wdb3@psu.edu

John M. Senko
University of Akron

Michael E. Bishop
Miami University

Hailiang Dong
Miami University

See next page for additional authors

Chemical Geology 283 (2011) 242–250

Contents lists available at ScienceDirect

Chemical Geology

journal homepage: www.elsevier.com/locate/chemgeo

Microbial reduction of chlorite and uranium followed by air oxidation

Gengxin Zhang [a], William D. Burgos [b,*], John M. Senko [c], Michael E. Bishop [d], Hailiang Dong [d], Maxim I. Boyanov [e], Kenneth M. Kemner [e]

[a] Institute of Tibetan Plateau Research, Chinese Academy of Sciences, Beijing, China
[b] Department of Civil and Environmental Engineering, The Pennsylvania State University, University Park, PA, USA
[c] Department of Geological and Environmental Sciences, University of Akron, Akron, OH, USA
[d] Department of Geology, Miami University, Oxford, OH, USA
[e] Biosciences Division, Argonne National Laboratory, Argonne, IL, USA

ARTICLE INFO

Article history:
Received 26 July 2010
Received in revised form 24 January 2011
Accepted 25 January 2011
Available online 3 February 2011

Editor: J. Fein

Keywords:
Smectites
Phyllosilicates
Uraninite
Iron reduction

ABSTRACT

To evaluate the stability of biogenic nanoparticulate U(IV) in the presence of an Fe(II)-rich iron-bearing phyllosilicate, we examined the reduction of structural Fe(III) in chlorite CCa-2 and uranium(VI) by *Shewanella oneidensis* MR-1, and the reoxidation of these minerals (after pasteurization) via the introduction of oxygen. Bioreduction experiments were conducted with combinations of chlorite, U(VI), and anthraquinone-2,6-disulfonate (AQDS). Abiotic experiments were conducted to quantify the reduction of U(VI) by chemically-reduced chlorite-associated Fe(II), the oxidation of nanoparticulate U(IV) by unaltered structural Fe(III) in chlorite, and the sorption of U(VI) to chlorite, to elucidate interactions between U(VI)/U(IV) and Fe(II)/Fe(III)-chlorite. Solids were characterized by X-ray diffraction, scanning electron microscopy, and X-ray absorption spectroscopy to confirm Fe and U reduction and reoxidation. U(VI) enhanced the reduction of structural Fe(III) in chlorite and nanoparticulate U(IV) was oxidized by structural Fe(III) in chlorite, demonstrating that U served as an effective electron shuttle from *S. oneidensis* MR-1 to chlorite-Fe(III). Abiotic reduction of U(VI) by chlorite-associated Fe(II) was very slow compared to biological U(VI) reduction. The rate of nanoparticulate U(IV) oxidation by dissolved oxygen increased in the presence of chlorite-associated Fe(II), but the extent of U(IV) oxidation decreased as compared to no-chlorite controls. In identical experiments conducted with bioreduced suspensions of nanoparticulate U(IV) and nontronite (another iron-bearing phyllosilicate), the rate of U(IV) oxidation by dissolved oxygen increased in the presence of nontronite-associated Fe(II). In summary, we found that structural Fe(III) in chlorite delayed the onset of U(VI) loss from solution, while chlorite-associated Fe(II) enhanced the oxidation rate of U(IV) by dissolved oxygen, indicating that chlorite-associated Fe(II) could not protect nanoparticulate U(IV) from oxygen intrusion but instead increased the oxidation rate of U(IV).

1. Introduction

Uranium contamination of sediment and groundwater is a problem at many U.S. Department of Energy (DOE) sites and uranium ore-processing sites where soluble U(VI) has migrated into groundwater. In aerobic groundwater, U(VI) carbonate complexes are often the predominant uranium species. These anionic or neutral U species tend to sorb weakly to solid phases and, therefore, can be relatively mobile in the environment (Akcay, 1998; Arnold et al., 1998). Under anoxic conditions U(VI) can be reduced to sparingly soluble U(IV) minerals and precipitated from groundwater (Lovley and Phillips, 1992). Bacterially mediated reduction of U(VI) to uraninite may be exploited for *in situ* remediation of uranium-contaminated sites (Lovley et al., 1991; Fredrickson et al., 2000; Brooks et al., 2003).

The stimulation of indigenous dissimilatory metal-reducing bacteria (DMRB) for uranium remediation is an area of active research at several DOE field sites. Assessment of the efficacy of any one strategy (e.g., ethanol addition) is typically based on changes in aqueous geochemistry measured in monitoring wells. Interpretation of these results is often challenging due to the complex suite of redox reactions potentially operative in these subsurface environments. For example, while the addition of an electron donor will promote reducing conditions, the availability of multiple electron acceptors (e.g., nitrate, Mn(III/IV) oxides, Fe(III) oxides, or sulfate) may enhance or impede U(VI) reduction. In a related manner, the concentration and flux of electron donor addition can also impact U(VI) reduction and U(IV) reoxidation (Tokunaga et al., 2008).

While considerable research has been conducted on uranium interactions with iron (oxyhydr)oxides (e.g., Jeon et al., 2005; Ginder-

* Corresponding author at: Dept. of Civil and Environmental Engineering, The Pennsylvania State University, 212 Sackett Building, University Park, PA 16802–1408, USA. Tel.: +1 814 863 0578; fax: +1 814 863 7304.
E-mail address: wdb3@psu.edu (W.D. Burgos).

0009-2541/$ – see front matter © 2011 Elsevier B.V. All rights reserved.
doi:10.1016/j.chemgeo.2011.01.021

Vogel et al., 2006), much less research has focused on uranium interactions with iron-bearing clay minerals (Stucki et al., 2007). Iron-bearing clay minerals are widely distributed in soils and sediments (Stucki et al., 2007) and often account for about half of the Fe mass in soils and sediments (Favre et al., 2006). Specifically, at the Old Rifle and Oak Ridge DOE field sites, the mass of iron associated with clay minerals is higher than the mass of iron associated with oxide minerals (Stucki et al., 2007; Komlos et al., 2008). In addition, chlorite is a common clay mineral at the DOE Hanford site (Schmeide et al., 2000; Baik et al., 2004; McKinley et al., 2007).

Compared to iron oxides which dissolve during reduction, the majority of reduced Fe(II) in iron-bearing clays is retained in the clay structure (Kostka et al., 1999; Dong et al., 2009). Fe(II) sorbed to mineral surfaces may be a more facile reductant compared to structural Fe(II) in clay minerals (Hofstetter et al., 2003, 2006), however, structural Fe(II) will not be flushed from a biostimulated reduction zone by advection. Thus, structural Fe(II) in clay minerals may be an important long-term reactant in maintaining anoxic conditions. The stability of U(IV) is, ultimately, the key criterion for determining success of any reductive immobilization strategy. The intrusion of oxidants such as oxygen or nitrate may be countered by a large reservoir of solid-phase reductants such as Fe(II)-bearing clay minerals.

In a recent, related study we measured the concomitant bioreduction of structural Fe(III) in the clay mineral nontronite and U(VI) by *Shewanella oneidensis* MR-1 (Zhang et al., 2009). From those experiments we found that uranium served as an effective electron shuttle to enhance the reduction of structural Fe(III) in nontronite but that delayed the onset of U(VI) loss from solution. In this current study, we not only report on the bioreduction of structural Fe(III) in the clay mineral chlorite CCa-2 and U(VI) but also measure the stability of bioreduced U(IV) in the presence of chlorite-associated Fe(II) and nontronite-associated Fe(II) upon oxygen intrusion. These two iron-bearing phyllosilicates were selected because they represent mineralogical end-members with respect to Fe(III) and Fe(II) content. Nontronite NAu-2 contains 4.2 mmol Fe/g with the majority of the structural iron as Fe(III) (Jaisi et al., 2007), while chlorite CCa-2 contains 3.4 mmol Fe/g with the majority of the structural iron as Fe(II). The objectives of this research were to study the interactions between U(VI) and the iron-rich ripidolite chlorite CCa-2 during their concomitant biological reduction, and then to further investigate the stability of bioreduced U(IV) and chlorite-associated Fe(II) in the presence of dissolved oxygen.

2. Experimental

2.1. Cell cultivation

S. oneidensis MR-1 was cultured in a chemically defined minimal medium as described previously (Burgos et al., 2008). Cells were harvested by centrifugation (15 min and 20 °C at 3,500 g), washed three times with anoxic 30 mM $NaHCO_3$ (pH 6.8, prepared under an 80:20% N_2:CO_2 atm) and resuspended in the same buffer.

2.2. Mineral preparation

CCa-2, an iron-bearing ripidolite chlorite from Flagstaff Hill (El Dorado County, CA, USA), was purchased in two separate batches from the Source Clays Repository (West Lafayette, IN). One batch was used for all the laboratory experiments and the second batch was used to produce a chlorite standard for Fe XANES. The chemical formula of this chlorite has been reported as $(Mg_{5.5}Al_{2.48}Fe^{2+}_{3.02}Fe^{3+}_{0.94}Ti_{0.01}Mn_{0.01})[(Si_{5.33}Al_{2.66})O_{20}](OH)_{16}$ as determined by electron microprobe analysis (Brandt et al., 2003). Clay fractions (0.5–2.0 μm) were suspended in 1 M NaCl for one week, separated in distilled water by centrifugation, washed repeatedly until no Cl^- was detected by silver nitrate, and then air-dried. The clay fractions were determined by XRD and SEM to be pure chlorite without other iron minerals. The iron content of CCa-2 has been reported to range from 17.6% (Brandt et al., 2003) to 34.5% (Jaisi et al., 2007). As determined by complete dissolution in HF/H_2SO_4, we measured an iron content of 18.8% (3.35 mmol Fe g^{-1}) for the chlorite used in all the experiments, and an iron content of 30.4% (5.42 mmol Fe g^{-1}) for the chlorite used for the Fe XANES standard. The Fe(II) content of CCa-2 has been reported to range from 46% (Fe(II)/total Fe) (Jaisi et al., 2007; Singer et al., 2009a, 2009b) to 76% (Brandt et al., 2003) to 86% (Keeling et al., 2000). As determined by an HF/H_2SO_4-phenanthroline assay (described below), we measured an Fe(II) content of 78% for the unaltered chlorite used in all the experiments, and an Fe(II) content of 55% for the unaltered chlorite used for the Fe XANES standard. CCa-2 is composed of a tetrahedral–octahedral–tetrahedral (TOT) layer attached to a brucite-like sheet (Brandt et al., 2003; Zazzi et al., 2006). According to a proposed structural model for CCa-2 (Brandt et al., 2003), 66% of the total Fe is located in the TOT layer and 34% of the total Fe is located in the brucite sheet, and all of the Fe(III) is located in the TOT layer (specifically in the octahedral sheet). The BET surface area of the air-dried chlorite was determined to be 25.4 m^2/g based on N_2 adsorption.

2.3. Bacterial reduction experiments

MR-1 bioreduction experiments were conducted in the presence or absence of U(VI), chlorite, or anthraquinone-2,6-disulfonate (AQDS) in 30 mM $NaHCO_3$ (pH 6.8) as described previously (Zhang et al., 2009). Chlorite CCa-2 was prepared in anoxic 30 mM $NaHCO_3$ buffer to produce a stock concentration of 100 g L^{-1}, and was sterilized by a 5-min exposure to microwave radiation (Keller et al., 1988). Chlorite and uranyl acetate were pre-equilibrated for two weeks before inoculation with MR-1. Experiments were conducted in 120 mL glass serum bottles where the chlorite concentration was 5.0 g L^{-1} (16.8 mM Fe_T, 22% Fe(III)), uranyl acetate concentrations ranged from 0 to 1.5 mM, and AQDS concentrations were either 0 or 0.10 mM depending on the experiment. MR-1 was inoculated at $0.5*10^8$ cells mL^{-1} (final concentration) with sodium lactate (5 mM) provided as the electron donor. After cells were added, reactors were periodically mixed and samples removed with sterile needle and syringe and HF/H_2SO_4-extractable Fe(II), ferrozine-extractable Fe(II), aqueous Fe(II), $NaHCO_3$-extractable U(VI), and aqueous U(VI) concentrations were measured as described below. All sample manipulations were performed inside an anoxic chamber (95:5% N_2:H_2 atm).

2.4. Experiments with U(VI) and chemically-reduced chlorite

Chlorite was reduced using the sodium citrate, bicarbonate, and dithionite (CBD) method as described by Stucki et al. (1984), and washed three times with anoxic distilled water (Hofstetter et al., 2003). CBD-reduced chlorite was dispensed into anoxic 30 mM $NaHCO_3$ buffer (pH 6.8) in 120 mL glass serum bottles (2.5 g L^{-1} final concentration, 8.4 mM Fe_T, 98% Fe(II)), and equilibrated at least 3 d before uranium addition (0.20 mM). Reactors were periodically mixed and samples removed to measure ferrozine-extractable Fe(II), aqueous Fe(II), $NaHCO_3$-extractable U(VI), and aqueous U(VI) concentrations.

2.5. Experiments with biogenic nanoparticulate U(IV) and unaltered chlorite

Biogenic nanoparticulate U(IV) precipitates were produced separately by MR-1, pasteurized (70 °C for 30 min), concentrated by centrifugation, and resuspended in anoxic 30 mM $NaHCO_3$ buffer (pH 6.8). Unaltered chlorite was dispensed into anoxic 30 mM $NaHCO_3$ buffer in 20 mL glass serum bottles (5.0 g L^{-1}, 16.8 mM Fe_T, 22%

Fe(III)) followed by the addition of 0.11 mM nanoparticulate U(IV). Reactors were periodically mixed and samples removed to measure ferrozine-extractable Fe(II), aqueous Fe(II), $NaHCO_3$-extractable U(VI), and aqueous U(VI) concentrations.

2.6. Experiments with bioreduced minerals and dissolved oxygen

Bioreduced suspensions containing combinations of U, chlorite, and AQDS were collected after a 21 d incubation period, pasteurized, concentrated by centrifugation, and then resuspended in anoxic 30 mM $NaHCO_3$ buffer at pH 6.8 in 20 mL glass serum bottles with 0.75 g L^{-1} bioreduced chlorite (2.5 mM Fe_T, 93% Fe(II)) and 0.15 mM U(IV). Oxygen was provided by flushing the headspace of anoxic $NaHCO_3$ buffer-containing serum bottles with filter-sterilized air as described previously (Burgos et al., 2008). Identical experiments were conducted with bioreduced suspensions of U, nontronite, and AQDS, except with 0.5 g L^{-1} bioreduced nontronite (2.1 mM Fe_T, 34% Fe(II)) and 0.15 mM U(IV). Reactors were periodically mixed and samples removed to measure ferrozine-extractable Fe(II), 0.5 N HCl-extractable Fe(II), aqueous Fe(II), $NaHCO_3$-extractable U(VI), and aqueous U(VI) concentrations.

2.7. Analytical techniques

Aqueous Fe(II) was measured after centrifugation for 10 min at 14,100 g and 20 °C, and analyzed using the ferrozine assay (Stookey, 1970). Ferrozine-extractable Fe(II) was measured after 0.1 mL of well-mixed suspension was added to 0.9 mL of anoxic ferrozine solution for 2 h, centrifuged, and analyzed using the ferrozine assay. HF/H_2SO_4-extractable Fe(II) was measured after samples were completely dissolved with 4.8% HF/2.16 N H_2SO_4 in a boiling water bath for 30 min, centrifuged, and analyzed using the 1,10-phenanthroline assay (Komadel and Stucki, 1988; Amonette and Templeton, 1998).

Aqueous U(VI) was measured after centrifugation for 10 min at 14,100 g and 20 °C. $NaHCO_3$-extractable U(VI) was measured in samples of well-mixed suspensions that were placed in 1 M anoxic $NaHCO_3$ (pH 8.4) (all sample collection and manipulations performed in anoxic glovebox) (Elias et al., 2003). After extraction for 1 h, solids were removed by centrifugation and U(VI) was measured in the supernatant. Measurements were done under ambient atmospheric conditions, so they are presumed to represent total U in the supernatant. U(VI) was measured by kinetic phosphorescence analysis on a KPA-11 (ChemChek Instruments, Richland, WA) (Brina and Miller, 1992). Adsorbed U(VI) was operationally defined as the difference between $NaHCO_3$-extractable and the initial aqueous U(VI) concentrations, divided by the chlorite concentration.

2.8. Mineralogical characterizations

Samples were analyzed by X-ray diffraction (XRD) and scanning electron microscopy (SEM) using previously described procedures (Zhang et al., 2007). Samples were analyzed by X-ray absorption spectroscopy (XAS) as described previously (Boyanov et al., 2007; Kemner and Kelly, 2007; Senko et al., 2007; Zhang et al., 2009). U L_{III}-edge EXAFS, U L_{III}-edge XANES and Fe K-edge XANES measurements were made at the Materials Research Collaborative Access Team (MRCAT/EnviroCAT) sector 10-ID beam line of the Advanced Photon Source at Argonne National Laboratory (ANL) (Segre et al., 2000). The XAS spectra were collected in transmission and fluorescence mode using quick-scanning of the monochromator. Energy calibration was maintained at all times by simultaneous collection of data from hydrogen uranyl phosphate (U edge) or metallic iron foil (Fe edge) using X-rays transmitted through the sample. An aqueous U(VI)–triscarbonato complex and a nanoparticulate $U^{(IV)}O_2$ solid were used as U EXAFS standards. Linear combination (LC) analysis of the U XANES spectra was performed using the following end-members: 1) U(VI) in a high carbonate solution at pH 11, speciation ~100% $UO_2(CO_3)_3$, and 2) a nanoparticulate $U^{(IV)}O_2$ standard produced from U(VI) by reduction with green rust (O'Loughlin et al., 2003). Similarly, the Fe XANES spectra were modeled by LC analysis using the following operational end-members: 1) an unaltered chlorite CCa-2 standard (55% Fe(II)), and 2) a fully reduced chlorite CCa-2 (98% Fe(II)). The fully reduced Fe(II)-CCa-2 standard was produced by CBD reduction (Stucki et al., 1984), and the Fe(II) contents of the standards were measured by the HF/H_2SO_4-phenanthroline assay (Komadel and Stucki, 1988).

3. Results

The speciation of Fe in these experiments is difficult to assign because of the multiple possible forms of Fe(II) in chlorite. In its unaltered, initial form, all of the Fe(III) in chlorite is structural Fe(III) located in the octahedral sheet of the TOT layer (Brandt et al., 2003). In its unaltered, initial form, the Fe(II) in chlorite is distributed in both the tetrahedral and octahedral sheets of the TOT layer and in the brucite-like sheet attached to the TOT layer. After chemical or biological reduction, additional Fe(II) should accumulate and be retained in the octahedral sheet of the TOT layer (site of Fe(III) reduction). However, depending on the extent of reduction and possible dissolution, Fe(II) may also exist as surface-complexed Fe(II) or interlayer-exchanged Fe(II). Operational extractions for Fe(II) from reduced phyllosilicates cannot readily distinguish between all these possible forms of Fe(II). In this study we have used centrifugation to measure soluble Fe(II), a ferrozine extraction as an attempt to measure surface-complexed Fe(II) and/or interlayer-exchanged Fe(II), and a HF/H_2SO_4-phenanthroline assay to measure total Fe(II). The difference between HF/H_2SO_4-phenanthroline and ferrozine extractable concentrations could be used to operationally define structural Fe(II) but, as discussed below, this becomes problematic due to analytical precision and the specificity of these extractants. Therefore, we have chosen the terms "structural Fe(III) in chlorite" to define a single, solid Fe(III) species (all in the octahedral sheet of the TOT layer) originally present in the unaltered material, and "chlorite-associated Fe(II)" to include multiple, solid-associated Fe(II) species — structural Fe(II) originally present in the unaltered material, newly formed structural Fe(II) in the octahedral sheet, surface-complexed Fe(II), and interlayer-exchanged Fe(II).

The speciation of reduced U(IV) in these experiments is also challenging to definitively assign because U(IV) may exist as uraninite, amorphous nanoparticulate U(IV), mononuclear U(IV) or some mixture of these phases (Bernier-Latmani et al., 2010; Fletcher et al., 2010). Based on SEM-EDS and XRD (Supplemental Material) of bioreduced suspensions, we found that amorphous uranium-rich nanoparticles were produced and predominated in the presence or absence of chlorite. The U L_{III}-edge EXAFS data from bioreduced U(IV) also indicate that the phases formed under our experimental conditions by *Shewanella* MR-1 were nearly identical in the presence or absence of chlorite, and consisted predominantly of nanoparticulate uraninite (Fig. 1). The EXAFS and Na HCO_3 extraction data on the bioreduced suspensions also suggested a lack of significant mononuclear U(IV) (discussed below). Therefore, we have chosen the terms "nanoparticulate U(IV)" or simply "U(IV)" to include all possible U(IV) species.

3.1. Bioreduction of U(VI) and structural Fe(III) in chlorite

S. oneidensis MR-1 was able to reduce both U(VI) and structural Fe(III) in chlorite when both of these terminal electron acceptors (TEAs) were present (Fig. 2). AQDS alone did not significantly enhance the reduction of structural Fe(III) in chlorite (Fig. 2a and c). We speculate that, because of the relatively high content of structural Fe(II) in chlorite, AH_2QDS cannot reduce structural Fe(III) in chlorite

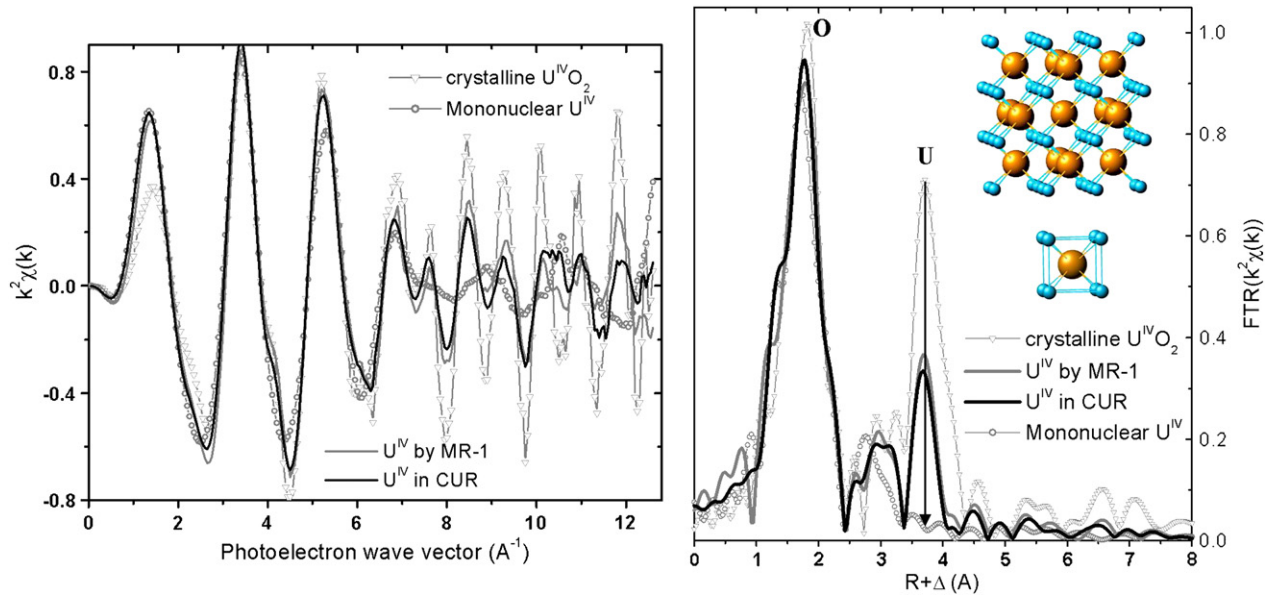

Fig. 1. U L_{III}-edge EXAFS data (left panel: $k^2\chi(k)$, right panel: Fourier transform) from biogenic U(IV) produced in the presence and absence of chlorite CCa-2 (data for the biogenic U(IV) in the absence of CCa-2 are from Burgos et al. (2008)). Data are compared to that from crystalline uraninite and biogenic mononuclear U(IV) (Fletcher et al. 2010). The inset in the right panel shows the molecular structure of a uraninite nanoparticle and the first coordination shell of U(IV). The contribution in the Fourier transformed spectra from the corresponding atoms are noted. The vertical arrow at ca. 3.5 Å shows the decrease in the U peak amplitude in the different phases.

due to a thermodynamic limitation. We do not believe that AH_2QDS was physically hindered from contacting structural Fe(III) in chlorite because we have previously shown that AQDS can enhance the bioreduction of structural Fe(III) in nontronite (Zhang et al., 2009). Similarly, other studies have shown that AQDS can enhance the rate and extent of reduction of iron oxides (Fredrickson et al., 2000; Zachara et al., 2002), manganese oxides (Fredrickson et al., 2002), smectite (Dong et al., 2003a), and illite (Dong et al., 2003b).

U(VI) alone and the addition of U(VI) + AQDS both enhanced the reduction of structural Fe(III) in chlorite, as evidenced by increased concentrations of aqueous Fe(II), ferrozine-extractable Fe(II), and HF/H_2SO_4-extractable Fe(II) (after 21 d). Measurements of total biogenic Fe(II) production are challenging in this system because of the high concentration of structural Fe(II) in the unaltered chlorite, the sorption of dissolved Fe(II) back onto the chlorite surface, and the oftentimes non-specific nature of some of the operational extractions. For example, we found that 0.5 N HCl did not efficiently extract all chlorite-associated Fe(II) while the HF/H_2SO_4 extraction did completely dissolve chlorite. Stucki et al. (2007) also reported that 0.5 N HCl was not reliable for the quantitative determination of Fe oxidation states in silicate minerals. Because of the high structural Fe(II) content in the unaltered chlorite, only relatively small changes in the large concentrations of HF/H_2SO_4-extractable Fe(II) can be measured in these experiments (Fig. 2d). In no-cell controls, no or very low concentrations of aqueous and ferrozine-extractable Fe(II) were produced and concentrations of HF/H_2SO_4-extractable Fe(II) remained essentially constant.

With respect to U(VI) reduction kinetics, the addition of chlorite increased the lag time before U(VI) was removed from solution and decreased the extent of U(VI) reduction after a 21 d incubation (Fig. 2b). The reduction of structural Fe(III) in chlorite appeared to compete with U(VI) reduction, and this is consistent with several other studies on the bioreduction of U(VI) in the presence of ferrihydrite (Wielinga et al., 2000), manganese oxides (Fredrickson et al., 2002), and nontronite (Zhang et al., 2009). In our recent experiments with U(VI) and nontronite (Zhang et al., 2009), we found that U served as an effective electron shuttle from *S. oneidensis* MR-1 to structural Fe(III) in nontronite, and that the lag phase for the onset of U(VI) loss from solution increased with increasing nontronite concentrations. The combined addition of chlorite + AQDS caused no lag in U(VI) reduction (compared to U(VI) alone), perhaps because of the stimulatory effect of AQDS on U(VI) reduction. U(VI) was not reduced in no-cell controls.

The sorption of U(VI) onto unaltered chlorite CCa-2 at pH 6.8 in anoxic 30 mM $NaHCO_3$ buffer was measured to quantify the distribution of U(VI) under the conditions used in the bioreduction experiments (Supplemental Material). With an initial U(VI) concentration of 0.10 to 1.5 mM, 17 to 4.0%, respectively, of the total U(VI) was sorbed onto unaltered chlorite (5.0 g L^{-1}) after 10 d (22 °C), with a maximum surface coverage of 0.54 μmol m^{-2}. These results are consistent with Singer et al. (2009a) who reported a U(VI) sorption extent to chlorite CCa-2 of 2.4 μmol m^{-2} at pH 6.5 with 0.1 mM dissolved carbonate (7 d, 23 °C). The higher bicarbonate concentration used in the current study likely suppressed U(VI) sorption to account for the lower value we report. U(VI) was not substantially reduced (<3%) by structural Fe(II) in the unaltered chlorite during our sorption experiments based on $NaHCO_3$-extractable U(VI) concentrations. This result is also consistent with Singer et al. (2009a) who reported that >95% of the U remained as U(VI) after sorption to chlorite. In U(VI) + chlorite no-cell controls prepared for our bioreduction experiments and analyzed after a 21 d incubation period, U(IV) contents of 3.0 ± 1.1% and 11 ± 10% were detected based on $NaHCO_3$ extraction and U XANES, respectively (Table 1, sample CUC).

The U L_{III}-edge EXAFS spectrum of the U(VI) + chlorite no-cell control (sample CUC) was similar to an aqueous U(VI)–triscarbonato complex, suggesting outer-sphere complexation of a U(VI)-carbonate anion to the chlorite surface (Supplemental Material). Based on this sorption mechanism, the aqueous tris-carbonato U(VI) complex was chosen as the U(VI) end-member for our XANES analysis. However, U(VI) sorption may cause an edge shift to lower energies, resulting in a XANES determination of 0% U(IV) (±10%) (Supplemental Material). Further evidence for the lack of U(VI) reduction in sample CUC is presented by the amplitude of the axial oxygen peak in the Fourier transformed EXAFS data, which was identical to that of the fully oxidized U(VI) standard (Supplemental Material). We conclude,

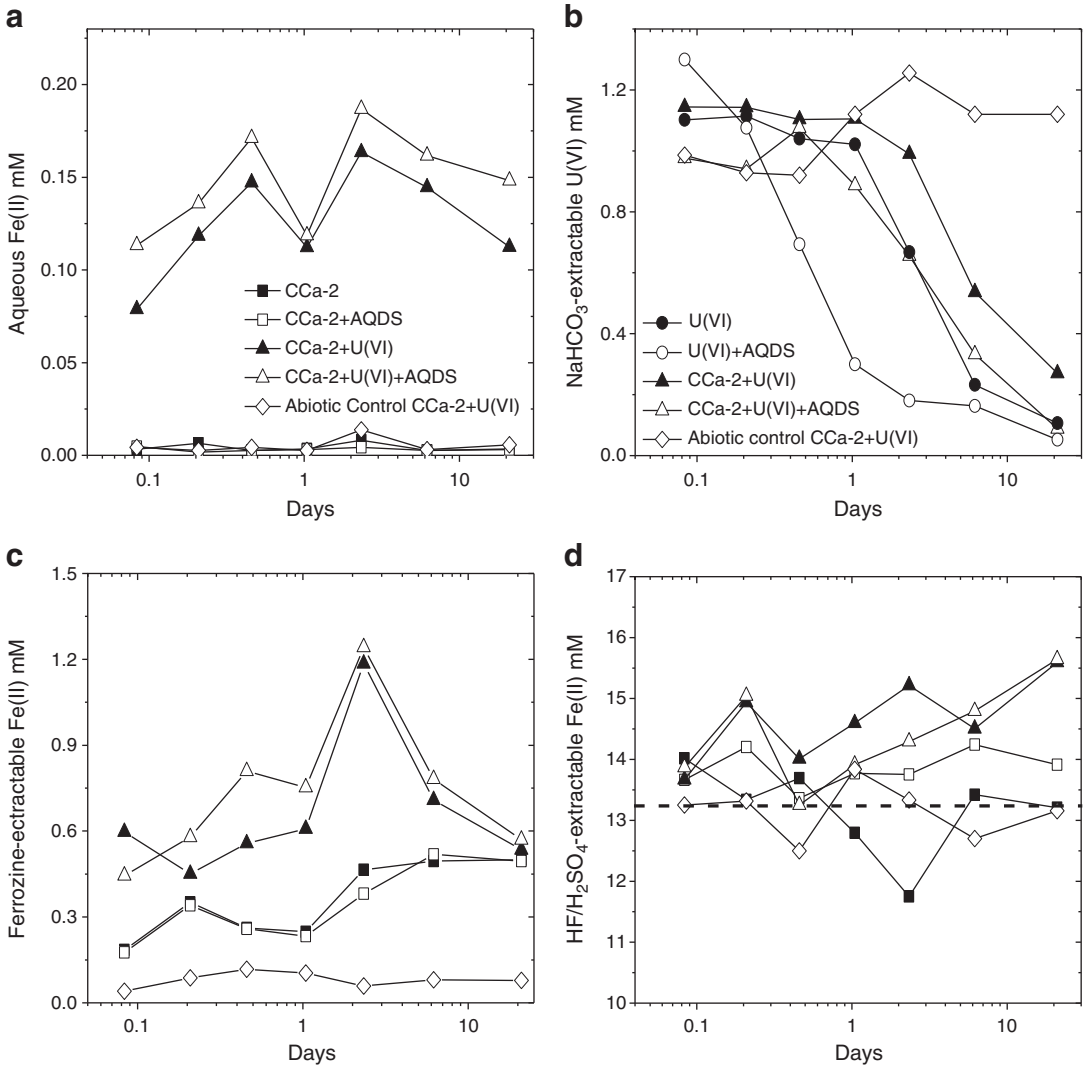

Fig. 2. Biological reduction of U(VI) and structural Fe(III) in chlorite CCa-2 by *S. oneidensis* MR-1 ($0.5*10^8$ cells mL^{-1}) in the presence or absence of AQDS (0.1 mM). Experiments were conducted with 1.0 mM U(VI), 5.0 g L^{-1} chlorite CCa-2 (16.8 mM Fe_T, 22% Fe(III)), and 5.0 mM lactate in 30 mM $NaHCO_3$ buffer, pH 6.8. (a) Aqueous Fe(II), (b) $NaHCO_3$-extractable U(VI), (c) ferrozine-exractable Fe(II), and (d) HF/H_2SO_4-extractable Fe(II). Dashed line in (d) represents starting concentration of structural Fe(II) in unaltered chlorite CCa-2. Symbols represent means of duplicate measurements.

Table 1
Average valence states of Fe and U within uranium–chlorite samples as determined by wet chemical methods and linear combination analysis of the XANES spectra. Sample names correspond to XANES spectra presented in Fig. 5.

Sample name/description	% Fe(II) in Chlorite		% U(IV) in precipitates	
	HF/H_2SO_4 dissolution	Fe K-edge XANES	$NaHCO_3$ extraction	U L_{III}-edge XANES
CUC 5 g L^{-1} Chlorite CCa-2 + 1 mM Uranyl(VI) acetate + 0 MR-1 (no-cell control) incubated for 21 d	78.3 ± 5.9	77 ± 10	3.0 ± 1.1	11 ± 10
CUR 5 g L^{-1} chlorite CCa-2 + 1 mM Uranyl(VI) acetate + $0.5*10^8$ cell mL^{-1} MR-1 incubated for 21 d	93.1 ± 1.3	99 ± 10	82.4 ± 9.0	99 ± 10
CUO CUR sample reacted with dissolved oxygen for 16 h	79.2 ± 1.0	82 ± 10	20.6 ± 9.6	56 ± 10

therefore, that with the materials and conditions used in these experiments, a very limited amount of U(VI) may be reduced by structural Fe(II) in unaltered chlorite but that this will not likely be an important process.

3.2. Abiotic reactions between U and chlorite

In addition to the biological reduction of U(VI) and structural Fe(III) in chlorite, abiotic reactions between U(VI) and structural Fe(II) in chlorite, between U(VI) and chlorite-associated Fe(II), and between U(IV) and structural Fe(III) in chlorite are all potentially operative. Based on sorption results and no-cell controls discussed above, the reduction of U(VI) by structural Fe(II) in the unaltered chlorite was very limited. Furthermore, in abiotic experiments conducted with chemically reduced chlorite, chlorite-associated Fe(II) displayed a limited ability to reduce U(VI) (Fig. 3a). For example, a significant loss of $NaHCO_3$-extractable U(VI) did not occur until after 30 h and decreased from 0.20 mM to 0.16 mM after 88 h of reaction with 2.5 g L^{-1} CBD-reduced chlorite (8.4 mM Fe_T, 98% Fe(II)). Because the aqueous U(VI) concentration remained essentially constant while the $NaHCO_3$-extractable U(VI) concentration decreased, we believe U(VI)

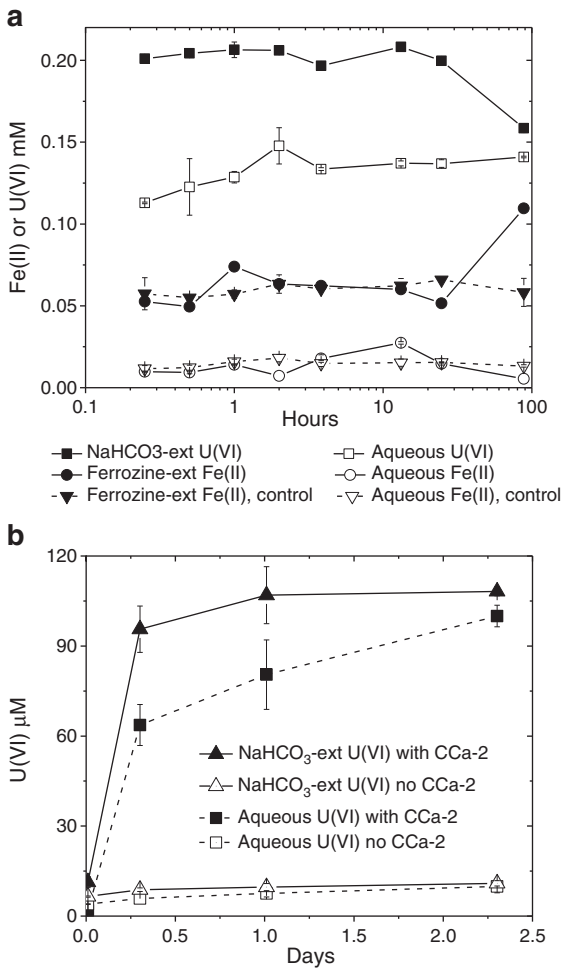

Fig. 3. Abiotic reactions between uranium and chlorite CCa-2. (a) Abiotic reduction of 0.20 mM U(VI) by chemically reduced chlorite CCa-2 (2.5 g L^{-1}, 8.4 mM Fe_T, 98% Fe(II)) in 30 mM $NaHCO_3$ buffer, pH 6.8. U(VI) was not added to the control. (b) Abiotic oxidation of biogenic nanoparticulate U(IV) (0.11 mM) by structural Fe(III) in unaltered chlorite CCa-2 (5.0 g L^{-1}, 16.8 mM Fe_T, 22% Fe(III)) in 30 mmol/L $NaHCO_3$, pH 6.8. Symbols and error bars represent means and standard deviations of duplicate measurements.

was first rapidly sorbed and then slowly reduced on the chlorite surface by chlorite-associated Fe(II). Aqueous Fe(II) remained constant in these experiments (Fig. 3a). In previous experiments conducted with 0.25 mM U(VI) and 2.5 g L^{-1} CBD-reduced nontronite (10.5 mM Fe_T, 27% Fe(II)) only a small fraction of U(VI) was reduced over an 83 d period (Zhang et al., 2009). The greater reduction extent of U(VI) by CBD-reduced chlorite as compared to CBD-reduced nontronite was likely due to the lower reduction potential of the fully reduced chlorite (i.e., higher Fe(II) content).

Abiotic experiments were also conducted to measure reaction kinetics between bioreduced (and pasteurized) nanoparticulate U(IV) and structural Fe(III) in unaltered chlorite. The U L_{III}-edge EXAFS data indicate that the bioreduced U(IV) phase consisted predominantly of nanoparticulate uraninite prior to pasteurization (Fig. 1). The amplitude of the U–U peak in data from U(VI) reduced by *Shewanella* MR-1 in the presence and absence of chlorite indicated a predominance of nanoparticulate uraninite in these systems. A linear combination fit with data from crystalline uraninite and mononuclear U(IV) did not reproduce our data well. The formation of non-uraninite U(IV) in our systems was unlikely because $NaHCO_3$ extraction of the bioreduced solids did not result in additional release of labile U(IV) phases (controls in Fig. 3b). Recent work has shown that biogenic non-uraninite U(IV) is more easily extractable than biogenic nanoparticulate uraninite (Alessi et al., 2010). Extracted U(IV) could then be oxidized to U(VI) prior to or during measurement by KPA. Previous studies found little to no Ostwald ripening of biogenic uraninite when incubated at 90 °C for 2 weeks (Singer et al., 2009b), suggesting that the 30 min pasteurization step did not alter the nanoparticulate U(IV) used in our reoxidation experiments.

Nanoparticulate U(IV) was effectively oxidized by structural Fe(III) in chlorite when reacted in anoxic 30 mM $NaHCO_3$ buffer (Fig. 2b). The production of U(VI) appeared to be pseudo-first order with respect to the remaining U(IV) concentration and all of the nanoparticulate U(IV) was reoxidized after ca. 2 d. Structural Fe(III) in chlorite oxidized nanoparticulate U(IV) at rates comparable to uraninite oxidation by poorly crystalline Fe(III) oxides (Senko et al., 2005; Ginder-Vogel et al., 2006) and by structural Fe(III) in unaltered nontronite (Zhang et al., 2009). U(IV) reoxidation kinetics were very rapid compared to U(VI) reduction by chlorite-associated Fe(II), demonstrating that the regeneration of U(VI) should enhance chlorite reduction through U valence cycling.

3.3. Reoxidation of nanoparticulate U(IV) and phyllosilicate-Fe(II) by dissolved oxygen

Experiments were conducted in which air was introduced into the headspace of bioreduced (and pasteurized) suspensions to initiate the reoxidation of U(IV) and chlorite-associated Fe(II). $NaHCO_3$-extractable U(VI) concentrations in the air-free controls (prepared with and without chlorite) were less than 7% of total U and never increased over the 16 h incubation (Fig. 4). The rate of nanoparticulate U(IV) oxidation (i.e., U(VI) production calculated over first 1–6 h) appeared to be pseudo-first order with respect to the remaining U(IV) concentration. Nanoparticulate U(IV) that was first produced in the presence of chlorite was subsequently oxidized more rapidly (based on first order rate constants) than nanoparticulate U(IV) first produced with U(VI) alone (Fig. 4a, Table 2). Nanoparticulate U(IV) that was first produced in the presence of chlorite was not subsequently completely oxidized, while nanoparticulate U(IV) first produced in the absence of chlorite was subsequently completely oxidized after 16 h (difference between series with square and triangle symbols in Fig. 4a). Only aqueous and ferrozine-extractable Fe(II) concentrations were measured for chlorite-containing suspensions in these experiments and revealed that chlorite-associated Fe(II) was subsequently oxidized simultaneously with U(IV) (data not shown).

When dissolved oxygen was introduced into this system, it could be consumed via the oxidation of nanoparticulate U(IV) or the oxidation of chlorite-associated Fe(II). If these processes were competitive, the rate of U(IV) oxidation would be expected to decrease in the presence of chlorite-associated Fe(II). If these processes were non-competitive, e.g., because of an excess of oxygen, then the rate of U(IV) oxidation would be expected to be unchanged by the presence of chlorite-associated Fe(II). Instead we found that the rate of U(IV) oxidation increased in the presence of chlorite-associated Fe(II) especially within the first hour of the experiment. Since structural Fe(III) in chlorite can rapidly oxidize nanoparticulate U(IV) (Fig. 3b), the "indirect" oxidation of U(IV) via chlorite-Fe(II/III) valence cycling could explain the observed increase in the rate of U(IV) oxidation in the presence of chlorite (Fig. 4a). Alternatively, prolonged solid–solid contact between chlorite and nanoparticulate U(IV) could facilitate solid-state galvanic coupling (Holmes and Crundwell, 1995; Klauber, 2008) which could also have the net effect of increasing the rate of U(IV) oxidation. While the first order rate constants for U(IV) oxidation increased in the presence of chlorite, the 16 h final extent of U(IV) oxidation decreased in the presence of chlorite. For example, 90–101% of the U(IV) produced in the absence of chlorite was reoxidized compared to 76–79% of the U(IV) produced in the presence of chlorite. The presence of chlorite-

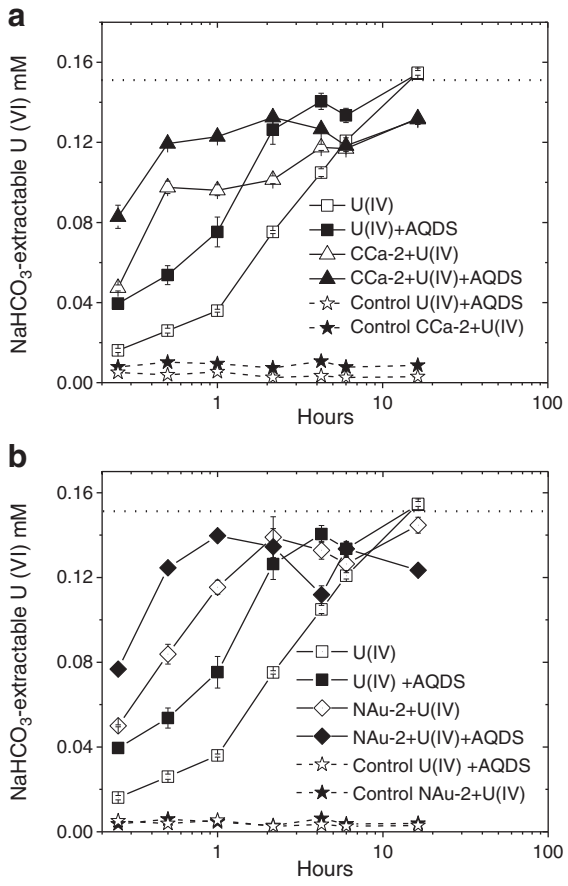

Fig. 4. Abiotic oxidation of biogenic nanoparticulate U(IV) and phyllosilicate-Fe(II) by dissolved oxygen in 30 mmol/L, $NaHCO_3$, pH 6.8. (a) Experiments initiated with 0.75 g L^{-1} bioreduced chlorite (2.5 mM Fe_T, 93% Fe(II)) and 0.15 mM U(IV). (b) Experiments initiated with 0.5 g L^{-1} bioreduced nontronite NAu-2 (2.1 mM Fe_T, 34% Fe(II)) and 0.15 mM U(IV). Air was not added to the controls. Symbols represent means of duplicate measurements. Dashed lines represent total U in suspensions.

associated Fe(II) may have protected U(IV) from complete oxidization.

To further examine the interactions between Fe(II)-bearing phyllosilicates, uraninite, and dissolved oxygen, we repeated these experiments with bioreduced (and pasteurized) suspensions of nontronite NAu-2 and U (Fig. 4b). With nontronite we were also able to accurately measure the oxidation kinetics of nontronite-associated Fe(II). Because of analytical precision issues associated with the HF/H_2SO_4-phenanthroline assay, this was not feasible with chlorite CCa-2 (e.g., Fig. 2d). As with chlorite, we found that the presence of nontronite increased the first order rate constants for U(IV) oxidation (differences between series with square and triangle symbols in Fig. 4b). The rates of nontronite-associated Fe(II) oxidation were comparable to the rates of U(IV) oxidation and were not strongly influenced by the presence of U (Table 2). As with chlorite, the extent of U(IV) oxidation decreased in the presence of nontronite where 76–84% of the U(IV) was reoxidized.

Table 2
Rates of reoxidation of nanoparticulate U(IV) and chlorite, and reoxidation of nanoparticulate U(IV) and nontronite-associated Fe(II) by the introduction of dissolved oxygen. Rates were modeled as pseudo-first-order with respect to the remaining concentration of the reduced species (i.e., [U(IV)] or [nontronite-Fe(II)]), and are reported as pseudo-first order rate constants. The 16 h extent of oxidation is reported as [reduced species]/[total element]*100%. Chlorite CCa-2 and nontronite NAu-2 were used.

Sample name/ description as shown in Fig. 3	U(IV)		Fe(II)	
	k_U (h^{-1})	Reoxidation extent (%)	k_{Fe} (h^{-1})	Reoxidation extent (%)
U(VI)	0.26	101 ± 5.0	n.a.	n.a.
U(VI) + AQDS	0.80	90.1 ± 5.1	n.a.	n.a.
CCa-2 + U(VI)	2.5	79.4 ± 9.6	n.d.	n.d.
CCa-2 + U(VI) + AQDS	4.4	75.6 ± 1.6	n.d.	n.d.
NAu-2	n.a.	n.a.	2.5	87.0 ± 0.4
NAu-2 + U(VI)	1.8	84.2 ± 3.6	2.0	86.7 ± 0.2
NAu-2 + U(VI) + AQDS	4.0	75.7 ± 3.1	3.1	88.6 ± 0.2

n.a. — not applicable.
n.d. — not determined due to precision issues with HF/H_2SO_4-phenanthroline assay with chlorite CCa-2.

3.4. Mineralogical characterizations

XRD patterns from chlorite samples showed changes in the relative intensity of peaks (001, 002, 003 and 004) between unaltered and bioreduced chlorite (Supplemental Material), suggesting that bioreduction caused a slight change in the stacking structure (Kameda et al., 2007). SEM images also showed physical alterations and dissolution features in the bioreduced chlorites as compared to abiotic controls (Supplemental Material). Based on XRD patterns and SEM images, biogenic U(IV) was relatively amorphous and nanoparticulate and accumulated extracellularly from MR-1. The U L_{III}-edge EXAFS data from the bioreduced sample indicated that the U(IV) phase consists predominantly of nanoparticulate uraninite (Fig. 1), nearly identical to U(IV) solids produced by *Shewanella* MR-1 in the absence of chlorite (Burgos et al., 2008). SEM-EDS analyses revealed increased uranium content with bioreduced chlorite particles that was not observed after the same samples had been reacted with dissolved oxygen.

The average oxidation state of both U and Fe were determined by XANES for select samples collected during these experiments. XANES spectra were collected from no-cell controls (1.0 mM U(VI), 5.0 g L^{-1} unaltered chlorite, 78% Fe(II)) that had been incubated for 21 d (referred to as CUC), from a bioreduced suspension containing $0.5*10^8$ cell mL^{-1} MR-1 that had been incubated for 21 d (referred to as CUR), and from the bioreduced suspension after exposure to dissolved oxygen for 16 h (referred to as CUO). The U L_{III}-edge XANES spectrum for the bioreduced sample closely matched that of a U(IV) standard of nanoparticulate UO_2 (Fig. 5a and b). The U(IV)/U(VI) ratio was determined by LC analysis of the XANES spectra. For the CUR sample, the U reduction extent calculated as ([U(IV)]/{[U(IV)] + [U(VI)]}) was 99 ± 10%, and in agreement with our estimate of 82 ± 9% based on total U(VI) measured after 1 M $NaHCO_3$ extraction (Table 1). For the CUO sample, the U reduction extent was 56 ± 10% based on U XANES and 21 ± 10% based on $NaHCO_3$ extraction. We are uncertain about what caused the discrepancy between these two estimates but note that U reduction extents were consistently higher for U XANES as compared to $NaHCO_3$ extraction.

The Fe K-edge XANES spectrum for the bioreduced sample (CUR) was similar to the CBD-reduced chlorite standard (Fig. 5c and d). The no-cell control (CUC) and the bioreduced-then-reoxidized sample (CUO) were intermediate between the unaltered chlorite standard (55% Fe(II)) and the CBD-reduced chlorite standard (98% Fe(II)). For the CUR sample, the Fe reduction extent calculated as ([Fe(II)]/{[Fe(II)] + [Fe(III)]})) was 99 ± 10%, and in agreement with our estimate of 93 ± 1.3% based on total Fe(II) measured after HF/H_2SO_4 extraction. For the CUO sample, the Fe reduction extent was 82 ± 10% based on Fe XANES and 79.2 ± 1.0% based on HF/H_2SO_4 extraction.

4. Discussion

In these experiments with multiple TEAs, i.e., structural Fe(III) in chlorite, U(VI), and AQDS, the apparent utilization of TEAs is complicated by valence cycling of the TEAs themselves. For example, we have recently shown that U valence cycling increased the rate and

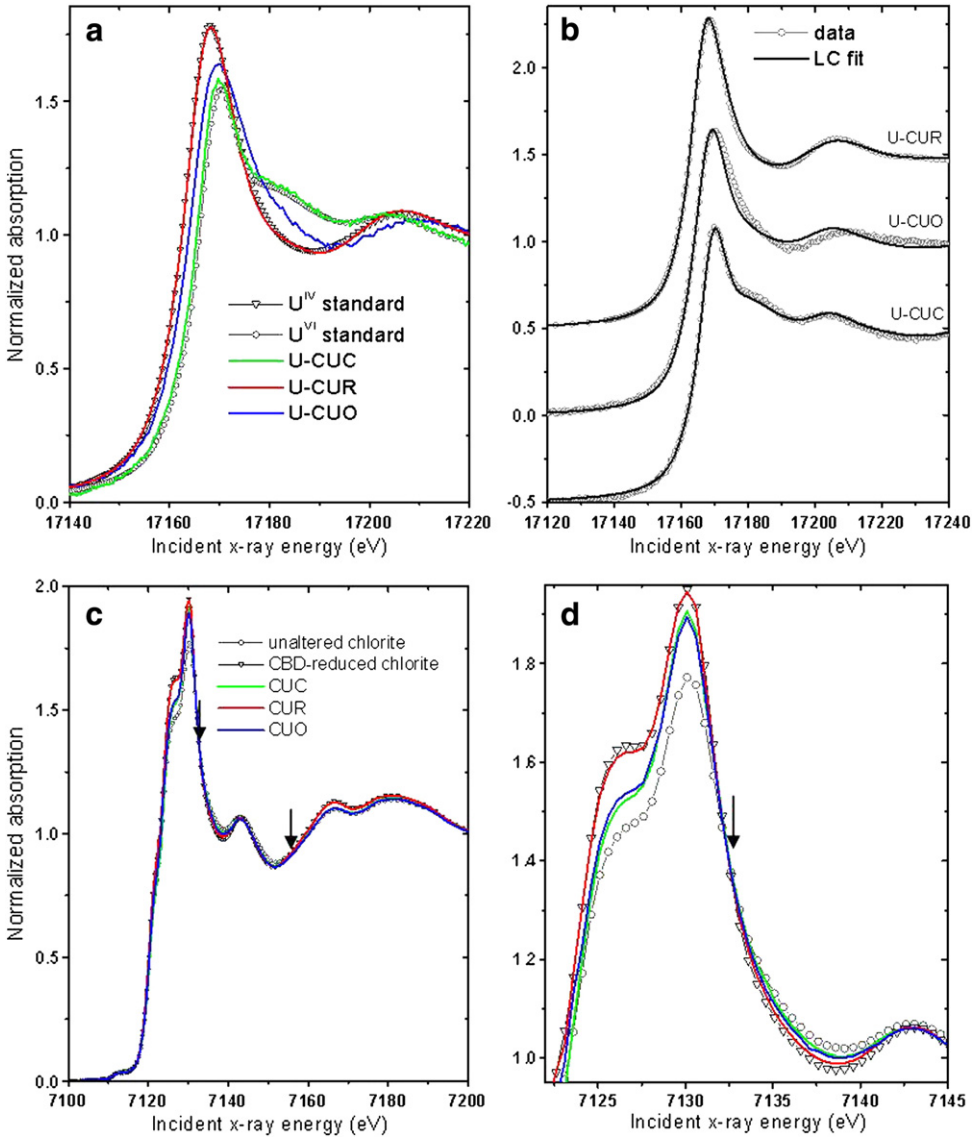

Fig. 5. (a) U L_{III}-edge normalized XANES spectra compared to U standards. U(VI) standard is $UO_2(CO_3)_3$(aq) and U(IV) standard is nanoparticulate uraninite. (b) Linear combination fit (line) of each U L_{III}-edge spectrum (symbols) where spectra are offset vertically for clarity. Numerical results are presented in Table 1. (c) Normalized Fe K-edge XANES spectra compared to Fe standards. The unaltered chlorite-Fe(II/III) standard is shown with circular symbols, and the CBD-reduced chlorite-Fe(II) standard is shown with triangular symbols. The samples shown are: CUC — 5 g L^{-1} chlorite CCa-2, 1 mM uranyl(VI) acetate, no cells and incubated for 21 days; CUR — 5 g L^{-1} chlorite CCa-2, 1 mM uranyl(VI) acetate, $0.5*10^8$ cell mL^{-1} MR-1 and incubated for 21 days; CUO — the CUR sample reacted with dissolved oxygen for 16 h. Isosbestic points are indicated by arrows. (d) Finer detail of the Fe XANES region.

extent of bioreduction of structural Fe(III) in nontronite (Zhang et al., 2009). In those experiments, substantial concentrations of biogenic Fe(II) evolved before any U(VI) was removed from solution even though U(VI) reduction (coupled to $U^{(IV)}O_{2(s)}$ oxidation) was essentially driving the reduction of structural Fe(III) in nontronite. Based on thermodynamic calculations using a reported standard-state reduction potential (E^0) value for nontronite (Jaisi et al., 2007), we showed that the apparent loss of U(VI) from solution would begin when sufficient Fe(II) had accumulated in the system (Zhang et al., 2009). Increasing Fe(II) concentrations decreased the redox potential of the structural Fe(III) in nontronite such that $U^{(IV)}O_2$(s) could not be reoxidized, at which point U valence cycling ceased. Because there are no reported E^0 values for chlorite, analogous thermodynamic calculations cannot yet be performed with the chlorite–uranium system.

The long-term success of *in situ* reductive immobilization of uranium hinges on the stability of U(IV) precipitates when eventually exposed to oxic groundwater. The stability of U(IV) species could be increased in highly reduced sediments if dissolved oxygen preferentially reacted with other reduced species (e.g., Fe(II) and S(−II)) before reacting with U(IV). At several uranium-contaminated DOE sites, iron-bearing phyllosilicates are more abundant than iron oxides and, in their Fe(II) state, could provide a substantial redox buffer to incoming oxidants. However, from these current experiments we have found that structural Fe(III) in chlorite delays the onset of U(VI) loss from solution, and chlorite-associated Fe(II) enhances the oxidation of U(IV) by dissolved oxygen. Although these findings may be a cause for concern, the inhibition of complete U(IV) reoxidation in the presence of chlorite (Fig. 5a) may enhance remediation efforts. Further studies are required to elucidate these processes.

Acknowledgements

This research was supported by the Subsurface Biogeochemical Research (SBR) Program, Office of Science (BER), U.S. Department of Energy (DOE) grant no. DE-SC0005333 to The Pennsylvania State

University, and by the National Science Foundation under grant no. CHE-0431328. ANL contributions were supported, in part, by the ANL Subsurface Science Scientific Focus Area project, which is part of the SBR Program of BER, U.S. DOE under contract DE-AC02-06CH11357. Use of the MRCAT/EnviroCAT sector at the Advanced Photon Source (APS) was supported by the U.S. DOE, Office of Science and the MRCAT/EnviroCAT member institutions. We thank S. D. Kelly, B. Ravel, and the MRCAT/EnviroCAT staff for assistance with XAS data collection at the MRCAT/EnviroCAT. Use of the APS was supported by the U.S. Department of Energy, Office of Science, Office of Basic Energy Sciences, under contract DE-AC02-06CH11357.

Appendix A. Supplementary data

Supplementary data to this article can be found online at doi:10.1016/j.chemgeo.2011.01.021.

References

Akcay, H., 1998. Aqueous speciation and pH effect on the sorption behavior of uranium by montmorillonite. J. Radioanal. Nucl. Chem. 237 (1–2), 133–137.
Alessi, D., Uster, B., Veeramani, H., Stubbs, J., Lezama-Pacheco, J., Bargar, J.R., Bernier-Latmani, R., 2010. Method to estimate the contribution of molecular U(IV) to the product of U(VI) reduction. Geochim. Cosmochim. Acta 74 (12), A11.
Amonette, J.E., Templeton, J.C., 1998. Improvements to the quantitative assay of nonrefractory minerals for Fe(II) and total Fe using 1, 10-phenanthroline. Clays Clay Miner. 46 (1), 51–62.
Arnold, T., Zorn, T., Bernhard, G., Nitsche, H., 1998. Sorption of uranium(VI) onto phyllite. Chem. Geol. 151 (1–4), 129–141.
Baik, M.H., Hyun, S.P., Cho, W.J., Hahn, P.S., 2004. Contribution of minerals to the sorption of U(VI) on granite. Radiochim. Acta 92 (9–11), 663–669.
Bernier-Latmani, R., Veeramani, H., Vecchia, E.D., Junier, P., Lezama-Pacheco, J.S., Suvorova, E.I., Sharp, J.O., Wigginton, N.S., Bargar, J.R., 2010. Non-uraninite products of microbial U(VI) reduction. Environ. Sci. Technol. 44 (24), 9456–9462.
Boyanov, M.I., O'Loughlin, E.J., Roden, E.E., Fein, J.B., Kemner, K.M., 2007. Adsorption of Fe(II) and U(VI) to carboxyl-functionalized microspheres: The influence of speciation on uranyl reduction studied by titration and XAFS. Geochim. Cosmochim. Acta 71 (8), 1898–1912.
Brandt, F., Bosbach, D., Krawczyk-Barsch, E., Arnold, T., Bernhard, G., 2003. Chlorite dissolution in the acid pH-range: a combined microscopic and macroscopic approach. Geochim. Cosmochim. Acta 67 (8), 1451–1461.
Brina, R., Miller, A.G., 1992. Direct detection of trace levels of uranium by laser-induced kinetic phosphorimetry. Anal. Chem. 64 (13), 1413–1418.
Brooks, S.C., Fredrickson, J.K., Carroll, S.L., Kennedy, D.W., Zachara, J.M., Plymale, A.E., Kelly, S.D., Kemner, K.M., Fendorf, S., 2003. Inhibition of bacterial U(VI) reduction by calcium. Environ. Sci. Technol. 37 (9), 1850–1858.
Burgos, W.D., McDonough, J.T., Senko, J.M., Zhang, G., Dohnalkova, A.C., Kelly, S.D., Gorby, Y.A., Kemner, K.M., 2008. Characterization of uraninite nanoparticles produced by *Shewanella oneidensis* MR-1. Geochim. Cosmochim. Acta 72 (20), 4901–4915.
Dong, H., Kostka, J.E., Kim, J.W., 2003a. Microscopic evidence for microbial dissolution of smectite. Clays Clay Miner. 51 (5), 502–512.
Dong, H., et al., 2003b. Microbial reduction of structural Fe(III) in illite and goethite by a groundwater bacterium. Environ. Sci. Technol. 37 (7), 1268–1276.
Dong, H., Jaisi, D.P., Kim, J., Zhang, G., 2009. Microbe–clay mineral interactions. Am. Mineral. 94, 1505–1519.
Elias, D.A., Senko, J.M., Krumholz, L.R., 2003. A procedure for quantitation of total oxidized uranium for bioremediation studies. J. Microbiol. Methods 53 (3), 343–353.
Favre, F., Stucki, J.W., Boivin, P., 2006. Redox properties of structural Fe in ferruginous smectite. A discussion of the standard potential and its environmental implications. Clays Clay Miner. 54 (4), 466–472.
Fletcher, K.E., Boyanov, M.I., Thomas, S.H., Wu, Q., Kemner, K.M., Loeffler, F.E., 2010. U(VI) reduction to mononuclear U(IV) by desulfitobacterium species. Environ. Sci. Technol. 44 (12), 4705–4709.
Fredrickson, J.K., Zachara, J.M., Kennedy, D.W., Duff, M.C., Gorby, Y.A., Li, S.M.W., Krupka, K.M., 2000. Reduction of U(VI) in goethite (α-FeOOH) suspensions by a dissimilatory metal-reducing bacterium. Geochim. Cosmochim. Acta 64 (18), 3085–3098.
Fredrickson, J.K., Zachara, J.M., Kennedy, D.W., Liu, C., Duff, M.C., Hunter, D.B., Dohnalkova, A., 2002. Influence of Mn oxides on the reduction of uranium(VI) by the metal-reducing bacterium *Shewanella putrefaciens*. Geochim. Cosmochim. Acta 66 (18), 3247–3262.
Ginder-Vogel, M., Criddle, C.S., Fendorf, S., 2006. Thermodynamic constraints on the oxidation of biogenic UO_2 by Fe(III) (hydr)oxides. Environ. Sci. Technol. 40 (11), 3544–3550.
Hofstetter, T.B., Schwarzenbach, R.P., Haderlein, S.B., 2003. Reactivity of Fe(II) species associated with clay minerals. Environ. Sci. Technol. 37 (3), 519–528.
Hofstetter, T.B., Neumann, A., Schwarzenbach, R.P., 2006. Reduction of nitroaromatic compounds by Fe(II) species associated with iron-rich smectites. Environ. Sci. Technol. 40 (1), 235–242.
Holmes, P.R., Crundwell, F.K., 1995. Kinetic aspects of galvanic interactions between minerals during dissolution. Hydrometallurgy 39, 353–375.
Jaisi, D.P., Dong, H.L., Liu, C.X., 2007. Influence of biogenic Fe(II) on the extent of microbial reduction of Fe(III) in clay minerals nontronite, illite, and chlorite. Geochim. Cosmochim. Acta 71 (5), 1145–1158.
Jeon, B.H., Dempsey, B.A., Burgos, W.D., Barnett, M.O., Roden, E.E., 2005. Chemical reduction of U(VI) by Fe(II) at the solid–water interface using natural and synthetic Fe(III) oxides. Environ. Sci. Technol. 39 (15), 5642–5649.
Kameda, J., Miyawaki, R., Kitagawa, R., Kogure, T., 2007. XRD and HRTEM analyses of stacking structures in sudoite, di-trioctahedral chlorite. Am. Mineral. 92 (10), 1586–1592.
Keeling, J.L., Raven, M.D., Gates, W.P., 2000. Geology and characterization of two hydrothermal nontronites from weathered metamorphic rocks at the Uley Graphite Mine, South Australia. Clays Clay Miner. 48 (5), 537–548.
Keller, M.D., Bellows, W.K., Guillard, R.R.L., 1988. Microwave treatment for sterilization of phytoplankton culture media. J. Exp. Mar. Biol. Ecol. 117 (3), 279–283.
Kemner, K.M., Kelly, S.D., 2007. In: Hurst, C.J. (Ed.), Synchrotron-based Techniques for Monitoring Metal Transformations, Third Edition. *Manual of Environmental Microbiology*. ASM Press, pp. 1183–1194.
Klauber, C., 2008. A critical review of the surface chemistry of acidic ferric sulphate dissolution of chalcopyrite with regards to hindered dissolution. Int. J. Miner. Process. 86 (1–4), 1–17.
Komadel, P., Stucki, J.W., 1988. Quantitative assay of minerals for Fe-2+ and Fe-3+ using 1, 10-phenanthroline. 3. A rapid photochemical method. Clays Clay Miner. 36 (4), 379–381.
Komlos, J., Peacock, A., Kukkadapu, R.K., Jaffe, P.R., 2008. Long-term dynamics of uranium reduction/reoxidation under low sulfate conditions. Geochim. Cosmochim. Acta 72 (15), 3603–3615.
Kostka, J.E., Haefele, E., Viehweger, R., Stucki, J.W., 1999. Respiration and dissolution of iron(III)-containing clay minerals by bacteria. Environ. Sci. Technol. 33, 3127–3133.
Lovley, D.R., Phillips, E.J.P., 1992. Bioremediation of uranium contamination with enzymatic uranium reduction. Environ. Sci. Technol. 26, 2228–2234.
Lovley, D.R., Phillips, E.J.P., Gorby, Y.A., Landa, E.R., 1991. Microbial reduction of uranium. Nature 350, 413–416.
McKinley, J.P., Zachara, J.M., Smith, S.C., Liu, C., 2007. Cation exchange reactions controlling desorption of Sr-90(2+) from coarse-grained contaminated sediments at the Hanford site, Washington. Geochim. Cosmochim. Acta 71 (2), 305–325.
O'Loughlin, E.J., Kelly, S.D., Cook, R.E., Csencsits, R., Kemner, K.M., 2003. Reduction of uranium(VI) by mixed iron(II/iron(III) hydroxide (green rust): formation of UO2 nanoparticles. Environ. Sci. Technol. 37 (4), 721–727.
Schmeide, K., Pompe, S., Bubner, M., Heise, K.H., Bernhard, G., Nitsche, H., 2000. Uranium(VI) sorption onto phyllite and selected minerals in the presence of humic acid. Radiochim. Acta 88 (9–11), 723–728.
Segre, C.U., Leyarovska, N.E., Chapman, L.D., Lavender, W.W., Plag, P.W., King, A.S., Kropf, A.J., Bunker, B.A., Kemner, K.M., Dutta, P., Duran, R.S., Kaduk, J., 2000. In: Pianetta, P. (Ed.), The MRCAT insertion device beamline at the Advanced Photon Source. *Synchrotron Radiation Instrumentation: Eleventh U. S. National Conference Vol. CP521*. American Institute of Physics, New York, pp. 419–422.
Senko, J.M., Mohamed, Y., Dewers, T.A., Krumholz, L.R., 2005. Role for Fe(III) minerals in nitrate-dependent microbial U(IV) oxidation. Environ. Sci. Technol. 39 (8), 2529–2536.
Senko, J.M., Kelly, S.D., Dohnalkova, A.C., McDonough, J.T., Kemner, K.M., Burgos, W.D., 2007. The effect of U(VI) bioreduction kinetics on subsequent reoxidation of biogenic U(IV). Geochim. Cosmochim. Acta 71 (19), 4644–4654.
Singer, D.M., Farges, F., Brown Jr., G.E., 2009a. Biogenic nanoparticulate UO2: synthesis, characterization, and factors affecting surface reactivity. Geochim. Cosmochim. Acta 73 (12), 3593–3611.
Singer, D.M., Mahera, K., Brown Jr., G.E., 2009b. Uranyl–chlorite sorption/desorption: evaluation of different U(VI) sequestration processes. Geochim. Cosmochim. Acta 73 (20), 5989–6007.
Stookey, L.L., 1970. Ferrozine—a new spectrophotometric reagent for iron. Anal. Chem. 42, 779–781.
Stucki, J.W., Golden, D.C., Roth, C.B., 1984. Effects of reduction and reoxidation of structural iron on the surface-charge and dissolution of dioctahedral smectites. Clays Clay Miner. 32 (5), 350–356.
Stucki, J.W., Lee, K., Goodman, B.A., Kostka, J.E., 2007. Effects of in situ biostimulation on iron mineral speciation in a sub-surface soil. Geochim. Cosmochim. Acta 71 (4), 835–843.
Tokunaga, T.K., Wan, J., Kim, Y., Daly, R.A., Brodie, E.L., Hazen, T.C., Herman, D., Firestone, M.K., 2008. Influences of organic carbon supply rate on uranium bioreduction in initially oxidizing, contaminated sediment. Environ. Sci. Technol. 42 (23), 8901–8907.
Wielinga, B., Bostick, B., Hansel, C.M., Rosenzweig, R.F., Fendorf, S., 2000. Inhibition of Bacterially Promoted Uranium Reduction: Ferric (Hydr)oxides as Competitive Electron Acceptors. Environ. Sci. Technol. 34 (11), 2190–2195.
Zachara, J.M., Kukkadapu, R.K., Fredrickson, J.K., Gorby, Y.A., Smith, S.C., 2002. Biomineralization of poorly crystalline Fe(III) oxides by dissimilatory metal reducing bacteria (DMRB). Geomicrobiol. J. 19 (2), 179–207.
Zazzi, A., Hirsch, T.K., Leonova, E., Kaikkonen, A., Grins, J., Annersten, H., Eden, M., 2006. Structural investigations of natural and synthetic chlorite minerals by X-ray diffraction, Mossbauer spectroscopy and solid-state nuclear magnetic resonance. Clays Clay Miner. 54 (2), 252–265.
Zhang, G., Dong, H., Kim, J., Eberl, D.D., 2007. Microbial reduction of structural Fe^{3+} in nontronite by a thermophilic bacterium and its roles in promoting the smectite to illite reaction. Am. Mineral. 92, 1411–1419.
Zhang, G., Senko, J.M., Kelly, S.D., Tan, H., Kemner, K.M., Burgos, W.D., 2009. Microbial reduction of iron(III)-rich nontronite and uranium(VI). Geochim. Cosmochim. Acta 73, 3523–3538.